Published in final edited form as:
J Phys Chem B. 2012 July 5; 116(26): 7644–7651. doi:10.1021/jp303778w.

Collisional Activation of $[14Pro+2H]^{2+}$ Clusters: Chiral Dependence of Evaporation and Fission Processes

Natalya Atlasevich[1], **Alison E. Holliday**[2,*], **Stephen J. Valentine**[1], and **David E. Clemmer**[1,*]
[1]Department of Chemistry, Indiana University, Bloomington, Indiana 47405

[2]Department of Chemistry and Biochemistry, Swarthmore College, Swarthmore, Pennsylvania 19081

Abstract

Ion mobility/mass spectrometry techniques are used to investigate the dissociation of the small proline cluster $[14Pro+2H]^{2+}$ produced by electrospray ionization. While this cluster is known to prefer heterochiral compositions (i.e., mixed L- and D-compositions, *J. Phys. Chem. A*, submitted for publication), it is possible to produce homochiral forms by electrospraying solutions containing only L or D proline. Differences in the measured cross sections for $[14Pro+2H]^{2+}$ produced from enantiomerically pure (100% L or 100% D) or racemic (50:50 L/D) solutions indicate that homochiral and heterochiral clusters have different structures. Upon low-energy collisional activation, both the heterochiral and homochiral doubly charged structures evaporate neutral proline monomers, resulting in the formation of $[xPro+2H]^{2+}$ ions, (where x = 13 to 9). At higher activation energies, there is evidence that these smaller clusters (primarily $[10Pro+2H]^{2+}$) fission to produce $[xPro+H]^{+}$ (where x = 1 to 6). Analysis of product ion intensities reveals a strong chiral preference associated with fissioning. Products of evaporation also show a chiral dependence, but to a lesser extent.

Keywords

ion mobility; proline; chirality; amino acid clusters; fragmentation; CID

Introduction

Recently, we reported that relatively small clusters of L- and D- proline (containing from 2 to 23 proline monomer units) display a remarkable oscillation in chiral preference.[1] Small, singly-protonated clusters $[xPro+H]^{+}$ (where x corresponds to the number of prolines) favor homochiral compositions for x = 4, 6, 11, and 12, and heterochiral compositions when x = 5 and 7. Larger doubly-protonated $[xPro+2H]^{2+}$ ions are preferentially homochiral for x = 18, 19, and 23, and favor mixed L/D compositions for x = 14, 16, 17, 20, 21, and 22. One might initially anticipate that, within a specific heterochiral preferring size, the L- and D- prolines are distributed homogenously throughout the cluster. However, it is difficult to rationalize the drastic changes in chiral preferences with size using such a model. Thus, we hypothesized that the origin of such oscillations might be attributed to pre-resolved assemblies within the heterochirally preferring clusters.[1] That is, the existence of L- and D- domains within a complex that has an overall heterochiral preference.

*Correspondence to: ahollid1@swarthmore.educlemmer@indiana.edu.

In this paper, we examine the dissociation mechanism for the $[14Pro+2H]^{2+}$ cluster. Specifically, we are interested in the influence of the precursor composition on fragment formation. The results presented below indicate that both the heterochiral and homochiral doubly charged structures evaporate neutral proline monomers, resulting in the formation of $[xPro+2H]^{2+}$ ions, (where x = 13 to 9). At higher activation energies, there is evidence that these smaller clusters fission to produce singly-protonated $[xPro+H]^{+}$ (where x = 1 to 6). Analysis of product ion intensities reveals a strong chiral preference associated with fissioning. As discussed below, we interpret such a finding as additional evidence for pre-resolved L- and D- domains within precursor states. Products of evaporation also show a chiral dependence, but to a lesser extent.

The present work is generally related to a larger effort to understand the origin of chiral systems.[4-9,14] Chirality is a characteristic feature of life.[2-6] Recently, several groups have focused investigations on simple chirally-selective systems, such as the formation of the magic number octamer cluster of serine.[7-14] Fragmentation of a singly-charged heterochiral serine octamer, ionized by an alkali metal cation, yields homochiral fragments.[15] This, along with our research on the composition of proline clusters,[1] points towards the likelihood of chirally resolved sub-structures within larger racemic systems. Thus, to obtain a true understanding of the chirality of a system, it is necessary to look not just at its overall composition, but also the intricacies of its formation and structure.

Dissociation of many different types of clusters, including atomic nuclei,[16] atomic clusters,[17,18] and peptide aggregates,[19] occurs by two competing processes: evaporation of neutral monomer subunits and fission into two or more fragments. This general phenomenon has been discussed since Rayleigh introduced his liquid drop model in 1882.[20] In this model, large droplets with fewer charges tend to dissociate by evaporation of neutral monomers. As many neutrals are lost, the smaller size of the droplet leads to an increase in the charge density on the cluster. The cluster fissions when the coulomb energy exceeds the attractive intermolecular forces holding it together.[17,19]

Clusters of amino acids show similarities with Rayleigh's ideas. Multiply charged serine[7,21-23] and serine-containing clusters,[24] and clusters of arginine,[25] tryptophan,[26] and the amino acid analog betaine[27-30] show predominant loss of neutrals for fragmentation of larger clusters and fission of smaller clusters with higher charge densities. The fission of multiply charged clusters is used to probe the structure and stability[8-9,30] of amino acid clusters and to distinguish doubly-charged clusters from singly charged clusters with identical *m/z*.[7,21] In a similar vein, fragmentation of larger multiply-charged clusters as a function of energy shows the loss of neutrals at lower fragmentation energies and fission at higher energies.[24,26,28] The present work aims to understand the role of chirality in these mechanisms.

Experimental

Overview

Ion mobility spectrometry mass spectrometry (IMS-MS) techniques, instrumentation, and theory have been described in detail previously.[31-42] Here, a brief description of the experimental approach used for the characterization of proline ion clusters is provided. Figure 1 shows a schematic diagram of the IMS-MS instrument used in the current studies. Proline cluster ions of the form $[xPro+nH]^{n+}$ (where x and n are the cluster order and charge state, respectively) are generated by ESI and introduced into a differentially-pumped desolvation region containing an hourglass ion funnel.[40] Ions are stored in the ion funnel and periodically (15 to 20 Hz) pulsed into the drift tube. The drift tube is ~289 cm long and is filled with ~3.0 Torr of He buffer gas (300 K). Ions separate in the drift tube according to

differences in their mobilities through the buffer gas under the influence of a weak uniform field (~10 V·cm^{-1}). The high-resolution drift tube depicted in Figure 1 has been described in detail previously.[43,44] Three ion funnels are placed at regular intervals within the drift tube in order to radially focus the diffuse ion cloud and increase overall ion transmission. Upon exiting the drift tube, ions enter the source region of an orthogonal-extraction time-of-flight (TOF) mass spectrometer and are pulsed into the field-free flight tube in order to obtain mass information. Because flight times in the evacuated flight tube are 10^2 to 10^3 times shorter than drift times (t_D) in the pressurized drift tube, it is possible to record the data using a high-efficiency nested approach that has been described previously.[37]

The drift times of specific ions can be used to obtain collision cross sections using the expression:[31]

$$\Omega=\frac{(18\pi)^{1/2}}{16}\frac{ze}{(k_bT)^{1/2}}\left[\frac{1}{m_I}+\frac{1}{m_B}\right]^{1/2}\frac{t_D E}{L}\frac{760}{P}\frac{T}{273.2}\frac{1}{N} \quad (1)$$

In Equation 1, ze, k_b, m_I, and m_B correspond to the ion's charge, Boltzmann's constant, the mass of the ion, and the mass of the buffer gas, respectively. The variables E and L correspond to the electric field in the drift tube and the drift length, respectively. P and T correspond to the buffer gas pressure and temperature, respectively. Finally, N is the neutral number density of the buffer gas at STP conditions.

IMS-IMS-MS dissociation experiments

Proline cluster ions $[14M+2H]^{2+}$ were mobility selected for collision-induced dissociation experiments. This was accomplished by applying a gating voltage to the second ion gate (G2 in Figure 1) at a specified delay time (~30 ms) with respect to the ion introduction pulse applied at the front of the drift tube. The gating pulse is ~80 s wide to allow only ions of a single mobility (or narrow range of mobilities) to be transmitted to the detector. Selected ions are then collisionally activated by applying a variable voltage to an ion activation region (IA2 in Figure 1) within the drift tube in what is referred to as the IMS-IMS-MS experiment. The t_D and m/z values of product ions are subsequently recorded as described above. One limitation of this IMS-IMS approach is that some clusters of different sizes have identical mobilities. The $[14Pro+2H]^{2+}$ cluster was chosen because it falls in a region of the spectrum where there is minimal overlap in drift time with other clusters. Some larger higher energy states are selected and activated. Because these clusters are low in abundance and fragments are found at different energies it is straight –forward to remove these contributions from the intensity profiles that we show below. Additionally, for the enantiopure solution, a limited amount of the $[13Pro+2H]^{2+}$ is co-selected because of overlapping drift times. The contribution from this species is also carefully accounted for in order to monitor fragmentation solely associated with the $[14Pro+2H]^{2+}$ ion. It is noted that these ions do not overlap in drift time at the selection time for the racemic solution.

Sample preparation

L- and D-proline (Fluka, 99 % purity), and deuterated L-proline ($HN(CD_2)_3CD)COOH$) (Cambridge Isotope Laboratories, Inc., ≥98% purity) were used without further purification, All proline solutions were prepared in 49:49:2 water:acetonitrile:acetic acid to a final concentration of 0.01 M. Proline solutions were pumped through a fused silica capillary tip at a flow rate of 0.1 μL min^{-1} using a syringe pump (KD Scientific). The capillary tip was made in-house (100μm i.d. x 360μm o.d., Polymicro) and was biased ~+2500 V above the ESI desolvation region entrance aperture.

Data analysis

Two-dimensional t_D(m/z) dot plots are generated using the Origin 8.6 software suite (OriginLab Corp., Northampton, MA). Intensities at specific t_D and m/z values are represented on a color scale. Software developed in-house is used to extract specific data points within the two-dimensional datasets in order to generate select drift time profiles. The software is also used to bracket t_D and m/z regions corresponding to specific cluster ions in order to integrate peak intensities.

Analysis of chiral preference of fragment ions

Chiral preference was determined using an isotopic labeling strategy demonstrated previously.[8] In this approach a mixture of deuterated L-proline and unlabeled D-proline is utilized. This allows the propensities of specific clusters to form mixed or resolved species to be measured directly. The intensity information of specific cluster compositions is compared with values that are calculated for a statistical distribution to determine if a preference exists. This analysis requires the comparison of x + 1 peaks (where x is the number of monomer units) to determine an overall preference for a specific cluster size. Although peaks associated with varying deuterated compositions for different cluster sizes overlap for large clusters, here the approach is used to determine the chiral preference of the small, singly charged fragments of specific clusters in order to obtain information regarding structural characteristics of larger clusters formed in solution.

Results and discussion

IMS-MS spectra

Figure 2 shows a two dimensional IMS-MS plot obtained by electrospraying 0.01 M solutions of enantiopure (100% L) and racemic (50:50 L/D) proline. As we have reported previously,[37] under the conditions of these experiments, ions separate into families depending upon the charge state and size of the cluster. From all solutions we observe a number of doubly charged clusters that range in size from $[9Pro+2H]^{2+}$ to $[27Pro+2H]^{2+}$. For the collisional activation studies presented below, we focus on the $[14Pro+2H]^{2+}$ ion. We choose this cluster size and charge state for several reasons. First, it is possible to form the $[14Pro+2H]^{2+}$ cluster from enantiomerically pure and racemic solutions. Second, this ion appears in a region of the spectrum (from both solutions) that is relatively uncongested. For the collisional activation studies, it is particularly important that there are no peaks immediately below the peak for the $[14Pro+2H]^{2+}$ ion. This makes it possible for us to infer the products of dissociation (as shown below). Finally, previous studies indicate that the $[14Pro+2H]^{2+}$ ion is slightly heterochirally preferring. Thus, dissociation of this ion to form smaller clusters that are homochirally preferring would suggest the existence of pre-resolved domains within the heterochiral precursors.

Figure 2 also shows an integrated slice of the drift time distribution (plotted on a cross section scale) for $[14Pro+2H]^{2+}$ ions formed from both solutions. From the differences in drift times, it is apparent that clusters formed from the enantiomerically pure L-proline solution are structurally different from those formed from racemic solutions. Specifically, the cross section for the heterochiral cluster is ~2% smaller than the value measured for the homochiral ion.

Collisional activation studies

Figure 3 shows drift time/mass spectra associated with selection and activation of the $[14Pro+2H]^{2+}$ ion. As shown in Figure 2, the $[14Pro+2H]^{2+}$ ion is located at a position in the two dimensional spectrum that makes it possible to select it in the G2 region with minimal interference from smaller clusters. Examples of the data obtained upon activation in the IA2

region are also shown in Figure 3. At relatively low activation voltages (50 V), we observe primarily loss of neutral monomers leading to the formation of the doubly-protonated $[13Pro+2H]^{2+}$ and $[12Pro+2H]^{2+}$ ions. When higher activation voltages are employed, much smaller, singly-charged clusters (e.g., $[5Pro+H]^{+}$, $[3Pro+H]^{+}$ and $[2Pro+H]^{+}$) are observed.

A summary of the intensities for all products that are produced by collisional activation is shown in Figure 4. Here, results for collisional activation studies of both the racemic and enantiopure samples are presented. Below, we discuss the fragmentation results for each sample and infer structural information regarding the $[14Pro+2H]^{2+}$ ions.

Because we have previously shown that the $[14Pro+2H]^{2+}$ cluster exhibits a heterochiral preference, it is instructive to consider the results obtained from the racemic mixture (Figures 4a and 4b). Upon increasing the activation voltage in the IA2 region of the instrument to 25 V, no significant fragmentation of the $[14Pro+2H]^{2+}$ ions is observed. Beginning at ~27 V, the $[14Pro+2H]^{2+}$ ions fragment via the loss of a single proline residue to form $[13Pro+2H]^{2+}$ ions (Figure 4a). This residue evaporation process continues to produce more $[13Pro+2H]^{2+}$ ions until reaching a maximum (~50% of the total ion signal) at ~50 V. Beyond this voltage the $[13Pro+2H]^{2+}$ ions begin to decrease and reach a minimum at ~70 V. It is noted that, just prior to the observation of the peak apex for the $[13Pro+2H]^{2+}$ ions, a new fragment corresponding to $[12Pro+2H]^{2+}$ ions is formed. This species is first observed at ~40 V, reaching an apex at ~60 V and a minimum at ~80 V. The data indicate that formation of these ions begins to compete with the formation of the $[13Pro+2H]^{2+}$ ions from the $[14Pro+2H]^{2+}$ species. This leads to the subsequent decrease in the $[13Pro+2H]^{2+}$ ions at higher activation voltages. This same pattern is observed for the smaller clusters as each begins to form and compete with the previous larger species. Therefore, the data show that successive neutral monomer losses are observed to form the $[12Pro+2H]^{2+}$, $[11Pro+2H]^{2+}$, $[10Pro+2H]^{2+}$, and $[9Pro+2H]^{2+}$ ions. The onset for the formation of each of these species is ~5 to 10 V above that of the larger size from which each originates.

Unlike the trends observed for the doubly-charged fragments, the singly-charged species are not produced in a successive, step-wise fashion; this indicates a different mechanism of dissociation (i.e., not evaporation). Dissociation to form singly-charged cluster ions does not occur until an activation voltage of ~60 V, commencing with the formation of the $[5Pro+H]^{+}$ species (Figure 4b). This cluster ion is observed to increase to a maximum of ~30% of the total ion intensity by ~100 V before decreasing to less than 10% by ~150 V. Interestingly, the $[6Pro+H]^{+}$ ions are formed only after increased activation voltage (~65 V) compared with the $[5Pro+H]^{+}$ species. These ions reach a maximum at ~90 V and are essentially not observed by ~110 V (Figure 4b). This trend is different from what is observed for the doubly-charged species, as the larger singly charged fragment cluster is formed only after employing higher activation voltages, suggesting that fragmentation of smaller doubly-charged cluster ions proceeds via fission. The $[4Pro+H]^{+}$ ions are observed to form at the same activation voltage as the $[6Pro+H]^{+}$ species. In comparison to the $[6Pro+H]^{+}$, these ions are formed in significantly higher abundance, reaching a maximum of ~22% of the total ion intensity by ~120 V. Additionally, unlike the $[6Pro+H]^{+}$ ions, these species persist to the highest voltage of ~150 V. Singly-charged clusters containing 2 and 3 proline residues are observed to initiate at ~75 V. Each of these species persists to the highest voltages, where they are near maximum values of ~8% and ~42% of the total ion intensity for the respective cluster ions. The $[Pro+H]^{+}$ ions are not formed until an activation voltage of ~110 V.

Overall, the trends from the fragmentation data indicated that the $[14Pro+2H]^{2+}$ ions fragment first to form smaller doubly-charged cluster ions by residue evaporation in a step-wise process. Reaching a critical cluster size (~10 proline residues) is required prior to formation of singly-charged cluster ions. As these ions are not formed in a step-wise process

and occur at varying activation voltages, it is suggested that the smaller doubly-charged ions undergo a fission type fragmentation to produce the singly-charged cluster ions.

Figures 4c and 4d show the fragmentation intensities for the same doubly- and singly-charged cluster ions formed during the study of the enantiopure sample. Interestingly, the fragmentation intensity profiles as a function of activation voltage are very similar for the doubly-charged ions. That is, the onset of fragmentation and intensity maxima are nearly the same for the $[13Pro+2H]^{2+}$, $[12Pro+2H]^{2+}$, $[11Pro+2H]^{2+}$, $[10Pro+2H]^{2+}$, and $[9Pro+2H]^{2+}$ ions, consistent with the neutral evaporation model of fragment ion formation. One exception is that the maximum intensity of $[12Pro+2H]^{2+}$ cluster ions comprises a significantly larger percentage of the total ion signal compared with what was observed for the racemic sample. It is instructive to consider that the $[12Pro+2H]^{2+}$ cluster ions have been shown to be homochirally preferring upon ESI of proline samples. That the intensity of this ion is significantly increased relative to the other doubly-charged species (as compared to the racemic sample) suggests that this fragmentation proceeds in a chirally dependent manner (see below for more discussion).

The collisional activation voltage dependence for the singly-charged cluster ions exhibits some differences when compared to the same ions formed upon analysis of the racemic sample. For example, the $[6Pro+H]^{+}$ ions are initially formed at lower activation voltages (~60 V). These ions also reach a much larger percentage of the total ion signal compared to their counterpart formed from the racemic solution. Similarly, the $[4Pro+H]^{+}$ reaches a greater maximum value even surpassing that of the $[5Pro+H]^{+}$ ions. These differences in singly-charged cluster ions produced by CID may provide some information regarding the specific structures of the $[14Pro+2H]^{2+}$ clusters. It can be argued from the data that the $[14Pro+2H]^{2+}$ clusters are formed from smaller clusters exhibiting specific chiral preferences. For example, from the racemic mixture, the constituent clusters that are homochirally preferring (i.e., the $[6Pro+H]^{+}$ and $[4Pro+H]^{+}$ species) are dramatically reduced compared with the relative abundances for the same species from the enantiopure solution. To further investigate this theory, it is informative to determine whether or not such clusters formed by precursor ion fragmentation exhibit the same chiral preference as the clusters of the same size formed in solution. To accomplish this we have performed fragmentation studies for a sample containing a mixture of unlabeled and isotopically labeled proline residues.

Isotopic analysis. As described above, for the isotope labeling study, a mixture of D-proline and deuterated L-proline is used. Clusters that incorporate deuterated prolines increase in mass by 7 for each L-proline residue. As mentioned above, the total number of peaks observed in the mass spectrum for a cluster of size x is x + 1. The relative intensity of each peak within the mass spectrum of a cluster is ratioed to the relative intensity expected from a statistical (binomial) incorporation of the deuterated L-proline.[8,9] Thus, if incorporation of proline shows no chiral preference, the ratios should all be approximately 1. Isotopically labeled data follow the pattern where flat, vee (V), and inverted vee (λ) distributions correspond to statistical, homochiral, and heterochiral preferences, respectively. It is assumed that if the larger clusters are formed from smaller clusters that exhibit chiral preference, these characteristics can be determined in the mass spectral pattern of the fragment ions. It is noted that the data in Figure 4 suggests that chiral preference is retained (see discussion above).

Figure 5 shows the chiral preferences that were obtained for the $[4Pro+H]^{+}$ $[5Pro+H]^{+}$, and $[6Pro+H]^{+}$ fragment ions. In general, the data show that the chiral preference exhibited by these clusters upon formation during the electrospray process is also observed for their counterparts formed by CID. It is instructive to consider the results for the $[6Pro+H]^{+}$ cluster

ions (Figure 5c). Previously, we have shown[1] that the propensity to form homochiral clusters is significantly greater than that to form any of the mixed clusters, as evidenced by the "V" distribution for the intensity ratio of each peak. This same distribution is observed for the cluster ions formed upon fragmentation of the larger, doubly-charged cluster. Not only do the fragment ions also exhibit a homochiral preference but also the magnitude of chiral preference is very similar. For example, for the $[6Pro+H]^+$ clusters formed in solution, the intensity ratio for the homochiral species is ~2.2 while that of all other cluster types is ~1.0 on average. Similar values of ~3.0 and ~1.0 are obtained for the same cluster types for those species formed upon ion activation. The intensity ratio patterns for the $[4Pro+H]^+$ and $[5Pro+H]^+$ cluster ions also exhibit similar patterns for those species formed directly from solution and those that are produced upon CID of larger cluster ions. That is, the intensity ratio profile of these clusters obtained by CID exhibit a "V" and "λ" pattern indicating homochiral and heterochiral preferences, respectively.

Mechanisms for chiral enrichment

The dissociation mechanism associated with the various cluster ions originating from a mixed L/D $[14Pro+2H]^{2+}$ cluster is summarized as a schematic in Figure 6. The chiral preferences of these clusters are known for ions produced from electrospray.[1] Although we use these preferences as a guideline, particularly in discussion of the chirality of doubly charged (evaporative) portion of the fragmentation pathway, we do not assume that formation and fragmentation are mirror image pathways (i.e. formation of all larger doubly charged clusters is not assumed to be from accretion of monomers onto the $[10Pro+2H]^{2+}$ cluster). For purposes of discussion, the $[14Pro+2H]^{2+}$ can be composed of 8L/6D proline residues and can also exist in a degenerate form composed of 8D/6L proline residues. For the discussion of the fragmentation mechanism, cluster degeneracy is not distinguished and so this cluster species is referred to as the 8/6 cluster ion. As previously determined, $[14Pro+2H]^{2+}$ is a heterochirally preferring cluster ion. Therefore it can be suggested that the cluster is primarily comprised of 8/6 and 7/7 proline residues. A smaller portion of the $[14Pro+2H]^{2+}$ may also contain 9/5 proline residues. Because $[13Pro+2H]^{2+}$ has been determined to be less heterochirally preferring than $[14Pro+2H]^{2+}$, it is suggested to be primarily composed of 8/5 and 7/6 proline residues. This occurs via evaporation of one of the proline enantiomers from the 8/6 and 7/7 species. Figure 6 shows that this process leads to a less heterochiral cluster.

In contrast to $[14Pro+2H]^{2+}$ and $[13Pro+2H]^{2+}$, the $[12Pro+2H]^{2+}$ cluster is observed to exist as a homochirally preferring cluster. As shown in Figure 6, the formation of such a species most likely proceeds via neutral evaporation from an 8/5 cluster to an 8/4 cluster. Additionally, a 7/5 composition could be formed as well as, to a lesser extent, a 9/3 composition. This idea is supported by the observation that the $[12Pro+2H]^{2+}$ cluster increases in abundance (Figure 4c) when it is generated from fragmentation in an enantiopure solution. Overall, Figure 6 suggests a pathway of fragment compositions associated with transitioning from heterochirally preferring ions to more homochirally preferring ions for the larger doubly-charged ions.

The formation of the $[11Pro+2H]^{2+}$ is observed to occur with another transition in chiral preference, as this species is observed to be slightly heterochirally preferring. This may occur as the $[12Pro+2H]^{2+}$ 8/4 and 7/5 compositions evaporate the majority enantiomer to form the 7/4 and 6/5 compositions for the $[11Pro+2H]^{2+}$. Evaporation of one proline residue from the $[11Pro+2H]^{2+}$ results in the formation of the $[10Pro+2H]^{2+}$. As noted previously, this cluster has a very small heterochiral preference. Indeed, there may be little chiral preference for this species. Therefore, it is inferred that the 5/5 and 6/4 compositions predominate the $[10Pro+2H]^{2+}$ cluster distribution.

The assumed $[10Pro+2H]^{2+}$ composition is further supported by products formed by cluster fission (Figure 4b). The data indicate that, in a racemic solution, the $[10Pro+2H]^{2+}$ ion fissions to initially form $[5Pro+H]^{+}$ ions at 55V (i.e., the $[5Pro+H]^{+}$ cluster predominates at lower activation voltages). The $[6Pro+H]^{+}$ and $[4Pro+H]^{+}$ product ions begin to form at ~65V immediately prior to the $[10Pro+2H]^{2+}$ cluster reaching its apex. This indicates that the $[6Pro+H]^{+}$ and $[4Pro+H]^{+}$ also originate predominantly from $[10Pro+2H]^{2+}$. While it is possible that other L/D compositions comprise the $[10Pro+2H]^{2+}$ ion, the majority of this cluster exists as either 5/5 or 6/4 species. Furthermore, while a small amount of $[9Pro+2H]^{2+}$ was formed during CID, this cluster is not considered in the proposed mechanism because it has a similar energy onset as the singly charged clusters discussed above.

By analyzing CID data for the isotopically labeled proline clusters (Figure 5), it is possible to infer L/D compositions for the singly charged fission products. The $[5Pro+H]^{+}$ isotopic distributions show the highest ratio of signal intensity for the 4/1 composition. This indicates that the 5/5 $[10Pro+2H]^{2+}$ clusters prefer to form $[5Pro+H]^{+}$ products composed of 4/1 prolines. A similar argument can be made for the $[6Pro+H]^{+}$ and $[4Pro+H]^{+}$ clusters, where the highest ratio of signal intensity is 4/0 for the $[4Pro+H]^{+}$ and 6/0 for the $[6Pro+H]^{+}$. This suggests that the 6/4 $[10Pro+2H]^{2+}$ cluster prefers to dissociate into 6/0 and 4/0 singly charged clusters. These results indicate that it is possible to form homochiral fission products from a mixed $[14Pro+2H]^{2+}$ L/D cluster, supporting the idea that pre-resolved domains exist within heterochiral $[14Pro+2H]^{2+}$ clusters.

Summary and Conclusions

The dissociation of the $[14Pro+2H]^{2+}$ ion has been examined with IMS-CID-IMS-MS techniques. In general, ion fragmentation is observed to proceed via proline residue evaporation to form smaller, doubly charged species ($[13Pro+2H]^{2+}$ to $[9Pro+2H]^{2+}$). This process occurs in a step-wise fashion with increasing collision activation voltage. At higher activation voltages, some of the smaller, doubly-charged cluster ions ($[11Pro+2H]^{2+}$ to $[9Pro+2H]^{2+}$) fission to produce singly-charged proline cluster ions. Examination of the abundance profiles as a function of activation voltage for product ions suggests the formation of chiral preferring species. Experiments involving the fragmentation of clusters of isotopically-labeled proline residues further confirm that product ions are chiral preferring and that the chiral preference of such species is similar to that of the cluster ions formed by direct ESI of proline solutions. Together, the data indicate that larger cluster ions are formed from chirally-resolved subunits.

Acknowledgments

The authors wish to acknowledge funding from the Indiana University MetaCyt initiative funded from the Lilly Endowment. Instrumentation used for this work is supported by a grant from the National Institute of Health (AG024547).

References

1. Holliday, A.; Atlasevich, N.; Myung, S.; Plasencia, MD.; Valentine, SJ.; Clemmer, DE. J. Phys. Chem. A. Submitted for publication to
2. Pasteur L. Ann. Phys. 1848; 24:442–459.
3. Bada JL, Luyendyk BP, Maynard JB. Science. 1970; 170:730–732. [PubMed: 5479627]
4. Pérez-García L, Amabilino DB. Chem. Soc. Rev. 2002; 31:342–356. [PubMed: 12491749]
5. Cintas P. Angew. Chem. Int. Ed. 2002; 41:1139–1145.
6. Nanita SC, Cooks RG. Angew. Chem. Int. Ed. 2006; 45:554–569.

7. Cooks RG, Zhang D, Koch KJ, Gozzo FC, Eberlin MN. Anal. Chem. 2001; 73:3646–3655. [PubMed: 11510829]
8. Julian RR, Hodyss R, Kinnear B, Jarrold MF, Beauchamp JL. J. Phys. Chem. B. 2002; 106:1219–1228.
9. Hodyss R, Julian RR, Beauchamp JL. Chirality. 2001; 13:703–706. [PubMed: 11746805]
10. Counterman AE, Clemmer DE. J. Phys. Chem. B. 2001; 105:8092–8096.
11. Koch KJ, Gozzo FC, Nanita SC, Takats Z, Eberlin MN, Cooks RG. Angew. Chem. Int. Ed. 2002; 41:1721–1724.
12. Takáts Z, Nanita SC, Cooks RG. Angew. Chem. Int. Ed. 2003; 42:3521–3523.
13. Yang P, Xu R, Nanita SC, Cooks RG. J. Am. Chem. Soc. 2006; 128:17074–17086. [PubMed: 17177460]
14. Perry RH, Wu C, Nefliu M, Cooks RG. Chem. Commun. 2007:1071–1073.
15. Nanita SC, Sokol E, Cooks RG. J. Am. Soc. Mass Spectrom. 2007; 18:856–868. [PubMed: 17346986]
16. Bohr N, Wheeler JA. Phys. Rev. 1939; 56:426–450.
17. Saunders WA. Phys. Rev. A. 1992; 46:7028–7041. [PubMed: 9908038]
18. Kruckeberg S, Schweikhard L, Dietrich G, Lutzenkirchen K, Walther C, Ziegler J. Chem. Phys. 2000; 262:105–113.
19. Jurchen JC, Garcia DE, Williams ER. J. Am. Soc. Mass Spectrom. 2003; 14:1373–1386. [PubMed: 14652186]
20. Lord Rayleigh FRS. Phil. Mag. 1882; 14:184–186.
21. Koch KJ, Gozzo FC, Zhang D, Eberlin MN, Cooks RG. Chem. Commun. 2001:1854–1855.
22. Nanita SC, Cooks RG. J. Phys. Chem. B. 2005; 109:4748–4753. [PubMed: 16851557]
23. Concina B, Hvelplund P, Nielsen AB, Nielsen SB, Liu B, Tomita S. J. Am. Soc. Mass Spectrom. 2006; 17:275–279. [PubMed: 16434210]
24. Kong X. J. Mass Spectrom. 2011; 46:535–545. [PubMed: 21630381]
25. Zhang D, Wu L, Koch KJ, Cooks RG. Eur. Mass. Spectrom. 1999; 5:353–361.
26. Feketeová L, Khairallah GN, Brunet C, Lemoine J, Antoine R, Dugourd P, O'Hair RA. J. Rapid Commun. Mass Spectrom. 2010; 24:3255–3260.
27. Feketeová L, O'Hair RA. J. Chem. Commun. 2008:4942–4944.
28. Feketeová L, O'Hair RA. J. Rapid Commun. Mass Spectrom. 2009; 23:3259–3263.
29. Wyer JA, Feketeová L, Nielsen SB, O'Hair RA. J. Phys. Chem. Chem. Phys. 2009; 11:8752–8758.
30. Yoo EJ, Feketeová L, Khairallah GN, O'Hair RA. J. Phys. Chem. A. 2011; 115:4179–4185. [PubMed: 21473600]
31. Mason, EA.; McDaniel, EW. Transport Properties of Ions in Gases. Wiley; New York: 1988.
32. St. Louis RH, Hill HH. Crit. Rev. Anal. Chem. 1990; 21:321–355.
33. Hoaglund Hyzer CS, Counterman AE, Clemmer DE. Chem. Rev. 1999; 99:3037–3079. [PubMed: 11749510]
34. Wittmer D, Luckenbill BK, Hill HH, Chen YH. Anal. Chem. 1994; 66:2348–2355.
35. von Helden G, Wyttenbach T, Bowers MT. Science. 1995; 267:1483–1485. [PubMed: 17743549]
36. Chen YH, Siems WF, Hill HH. J. Anal. Chim. Acta. 1996; 334:75–84.
37. Hoaglund CS, Valentine SJ, Sporleder CR, Reilly JP, Clemmer DE. Anal. Chem. 1998; 70:2236–2242. [PubMed: 9624897]
38. Hoaglund-Hyzer CS, Li J, Clemmer DE. Anal. Chem. 2000; 72:2737–2740. [PubMed: 10905301]
39. Bluhm BK, Gillig KJ, Russell DH. Rev. Sci. Instrum. 2000; 71:4078–4086.
40. Tang K, Shvartsburg AA, Lee HN, Prior DC, Buschbach MA, Li FM, Tolmachev AV, Anderson GA, Smith RD. Anal. Chem. 2005; 77:3330–3339. [PubMed: 15889926]
41. Revercomb HE, Mason EA. Anal. Chem. 1975; 47:970–983.
42. Wyttenbach T, von Helden G, Batka JJ, Carlat D, Bowers MT. J. Am. Soc. Mass Spectrom. 1997; 8:275–282.

43. Merenbloom SI, Koeniger SL, Valentine SJ, Plasencia MD, Clemmer DE. Anal. Chem. 2006; 78:2802–2809. [PubMed: 16615796]

44. Koeniger SL, Merenbloom SI, Valentine SJ, Jarrold MF, Udseth H, Smith RD, Clemmer DE. Anal. Chem. 2006; 78:4161–4174. [PubMed: 16771547]

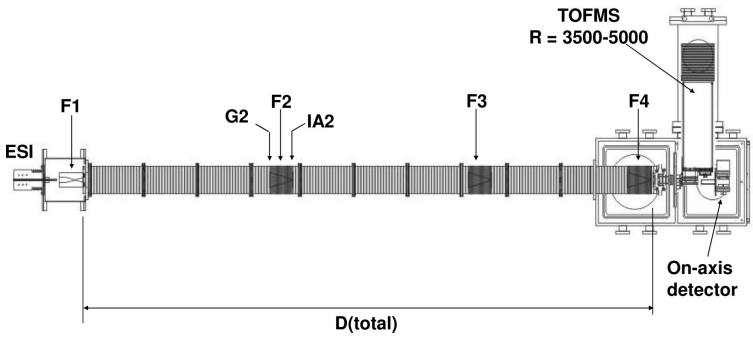

Figure 1.
Schematic of a prototype IMS-IMS-IMS-TOF instrument, where “F” corresponds to an ion funnel, “G” is the selection gate, and “IA” is an ion activation region. See text for more details.

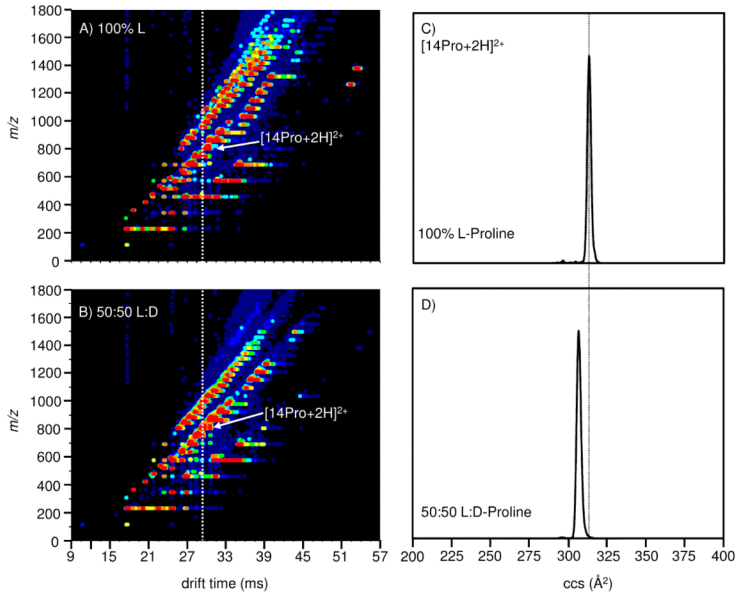

Figure 2.

Nested $t_D(m/z)$ plot for electrosprayed solutions of 0.01M (a) enantiopure (100% L) and (b) racemic (50:50 L/D) proline. The arbitrary intensity scheme represents the least intense features in navy and the most intense features in red. The collision cross section for the $[14Pro+2H]^{2+}$ cluster formed from the (c) enantiopure and (d) racemic solutions differ by ~2%.

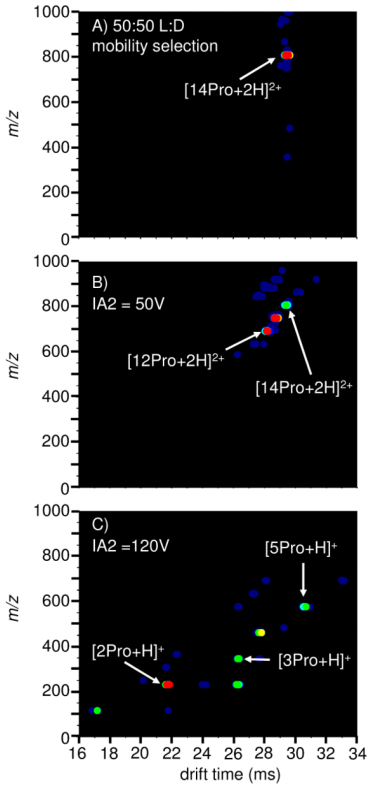

Figure 3.

A narrow distribution of $[14Pro+2H]^{2+}$ cluster formed from the 50:50 L/D solution is (a) mobility selected and activated with (b) 50V and (c) 120V in the IA2 region. At the relatively low activation voltage (50V), the $[14Pro+2H]^{2+}$ cluster evaporates neutral monomers. At the higher activation voltage (120V), the doubly charge clusters fission to produce singly charged proline clusters.

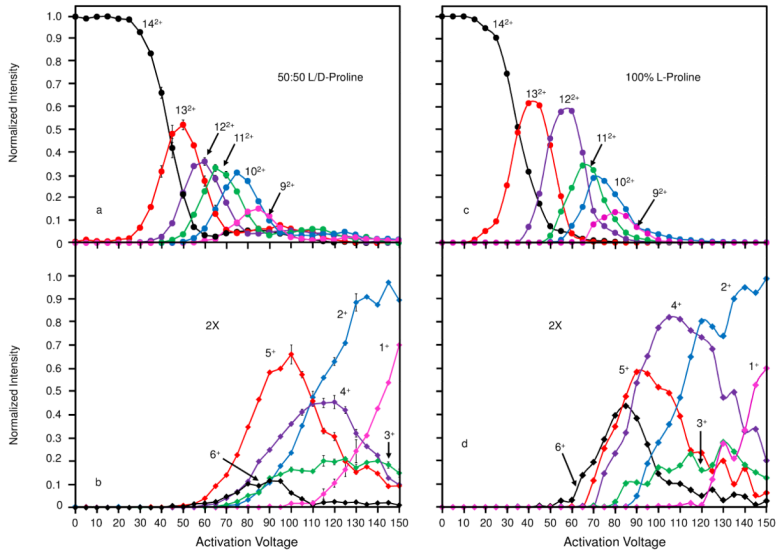

Figure 4.

Normalized intensity as a function of activation voltages (0-150V) are shown for the [14Pro +2H]$^{2+}$ cluster. Evaporation of neutrals (a) for the [14Pro+2H]$^{2+}$ cluster formed from the racemic solution produces [xPro+2H]$^{2+}$ where x = 9 to 13. At ~60V the doubly charged ions begin to fission (b) to form singly charged [xPro+H]$^{+}$ clusters where x = 1 to 6. (c) Evaporation and (d) fission of the homochiral [14Pro+2H]$^{2+}$ cluster electrosprayed from 100% L-proline solution is also shown. Normalized intensity for the singly charged clusters formed from both the racemic and enantiopure solutions are magnified by a factor of two for better comparison. Furthermore, activation curves for the homochiral [14Pro+2H]$^{2+}$ cluster are corrected to eliminate the dissociation byproducts of the [13Pro+2H]$^{2+}$ that is present in the mobility selection of the [14Pro+2H]$^{2+}$.

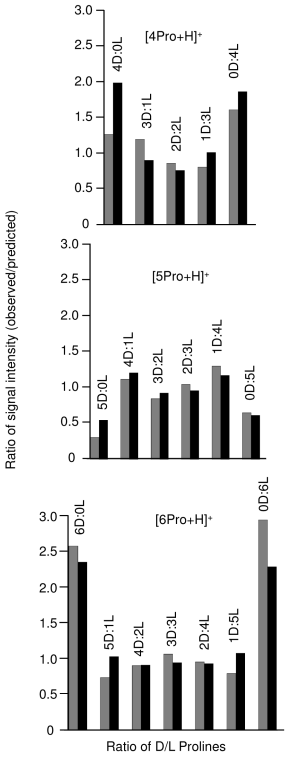

Figure 5.

Ratio of the observed to predicted (statistical) intensities for the proline clusters: $[4Pro+H]^+$, $[5Pro+H]^+$, and $[6Pro+H]^+$, where the *x* axis refers to the number of L/D prolines in the 50:50 D- and L- $[(HN(CD_2)_3CD)COOH]$ proline mixture. Grey bar graphs represent data obtained for the singly charged clusters formed by CID. Black bar graphs represent data obtained for the singly charged clusters formed during electrospray.

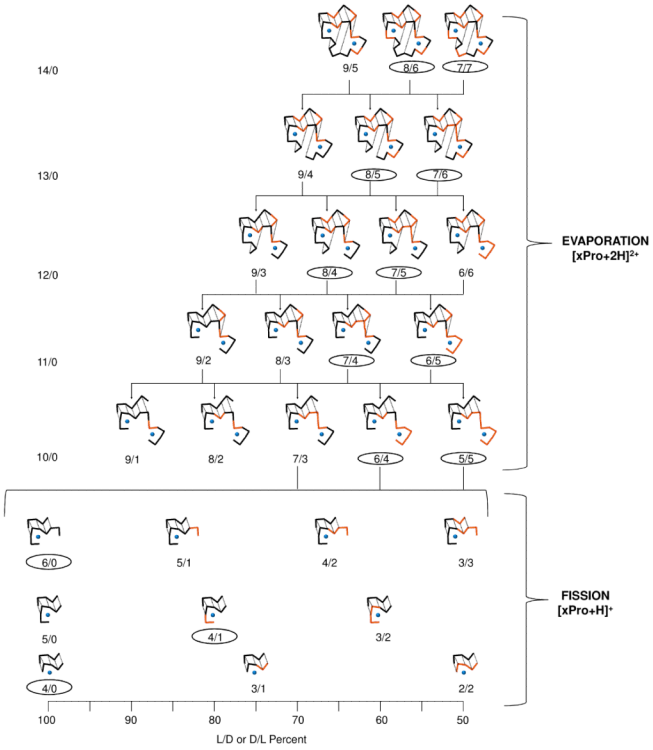

Figure 6.

A hypothetical schematic showing the dissociation scheme of the mixed L/D $[14Pro+2H]^{2+}$ cluster. The residue evaporation and ion fission regions of the fragmentation process are labeled. Cluster ion compositions are designated by the numbers of L- and D- proline residues as “L/D”. Composition degeneracies are not designated (see text for details). Circled compositions represent preferred fragmentation pathways (see preferred fragments in Figures 4 and 5).